Journal of
Mechanics of
Materials and Structures

# COMPUTATIONAL MODELING OF TUNGSTEN CARBIDE SPHERE IMPACT AND PENETRATION INTO HIGH-STRENGTH-LOW-ALLOY (HSLA)-100 STEEL TARGETS

Costas G. Fountzoulas, George A. Gazonas and Bryan A. Cheeseman

Volume 2, Nº 10 December 2007

mathematical sciences publishers

JOURNAL OF MECHANICS OF MATERIALS AND STRUCTURES
Vol. 2, No. 10, 2007

# COMPUTATIONAL MODELING OF TUNGSTEN CARBIDE SPHERE IMPACT AND PENETRATION INTO HIGH-STRENGTH-LOW-ALLOY (HSLA)-100 STEEL TARGETS

COSTAS G. FOUNTZOULAS, GEORGE A. GAZONAS AND BRYAN A. CHEESEMAN

The current investigation tested the existing material models of tungsten carbide and HSLA-100 steel by comparing available published experimental data, such as the depth and diameter of the impact crater, against the corresponding simulated results. Lagrange and smoothed particle hydrodynamics (SPH) simulations were carried out using an axisymmetric model of the tungsten carbide (WC) projectile and the HSLA-100 target. The Lagrange simulation predicted the crater diameter accurately. The SPH simulation efforts predicted the crater diameter with acceptable accuracy (within 15%) for impact velocities ranging from 830 to 2550 m/s. However, the SPH simulations failed to predict the crater depth for impact velocities greater than 1.5 km/s. The current paper will detail the results of parametric studies conducted using various existing models in an attempt to simulate the observed damage and the efforts to improve the simulation prediction of the experimental data.

## 1. Introduction

Impact and penetration problems include but are not limited to, armor and antiarmor development, personnel armor, vehicle protection, and analysis of weapon design. Multiple physical phenomena are involved during penetration, such as fracture, failure, residual stresses, and friction heating. Sufficient knowledge of the material response to these dynamic phenomena and consequent development of material models which can depict accurately the behavior of the materials are required for the design of efficient structures under high rate loadings. However, to include underlying physics in the model is a difficult task. In reality, since empirical and analytical approaches cannot capture all of these phenomena, numerical simulation has become a necessary tool for the study of these phenomena. Smoothed particle hydrodynamics (SPH) is a meshless Lagrangian technique, and can model large material shear flows and material fracture more robustly. The deficiencies of the conventional finite element methods involve large mesh distortions and mesh-size sensitivity. Furthermore, the production of large local inelastic flow and material cracking during the penetration process generate irrecoverable mesh distortions. The mesh-size sensitivity problem stems from the inability of conventional continuum constitutive models to treat material softening during failure. Meshless methods, such as SPH, applied to penetration problems have achieved only limited success due to an inherent tensile instability and inability to reproduce low-order polynomials. However, recent advances in meshless technology have addressed these shortcomings, and have overcome many other difficulties in failure simulation, boundary conditions, and efficiency (see www.ca.sandia.gov/8700/projects/content.php?cid=100).

*Keywords:* computational modeling, Lagrange, smoothed particle hydrodynamics (SPH), meshless particles, AUTODYN, tungsten carbide, HSLA-100 steel, impact.

HSLA-100 steel is an improved weldability steel, which has been used to replace high strength alloy steels in a number of applications, including aircraft carriers, cruisers, and submarines. Modern warships, surface combatants and submarines, require high strength steel plate in increasing portions of the hull structure for weight reduction, better stability, increased payload, increased mobility, and survivability [Czyryca et al. 2003]. According to Czyryca et al. [2003],

> Nearly half of the total Department of Defense requirement for alloy and armor steel plate is used in naval shipbuilding. In service, naval ship structures are subjected to a complex spectrum of loads and environments, and the structural steels and welding materials used in hull fabrication must demonstrate high fracture toughness for these extreme conditions. The routine dynamic loads in service include wave loading, sea slap, slamming, vibration, cargo buoyancy, and aircraft landing. Thus, the key requirements for naval shipbuilding steels are not only strength, weldability, and toughness at low temperature under shock events, but are also driven by economics, in order to keep an affordable ship acquisition cost.

HSLA-100 is a high yield strength, high toughness, and improved weldability steel, used as an alternative to quenched and tempered alloy steels [Martineau et al. 2004]. Tungsten carbide (WC) accounts for about 65% of tungsten consumption in the USA each year (see www.mii.org/Minerals/phototung.html).

It is combined with cobalt as a binder to form the so-called cemented carbides, which are used in cutting and wear applications. Most of these carbides have characteristically high hardness, good electrical and thermal conductivity, and high stability. These properties account for the principal applications: structures resistant to chemical reaction, uses in which wear resistance is of major importance, and high-temperature radiant-energy sources. The brittleness of carbides, however, has prevented their use as single-phase materials in highly stressed structural applications and has led to the development of metal-bonded composites (cemented carbides or cermets); see www.itia.org.uk/tungsten/tungsten_facts.html.

Ceramics are materials that possess characteristics such as low density, high hardness, and high compressive strength which make them ideal for use in light weight armor; however, ceramics are also brittle and have a low tensile strength, which complicates the design of such systems. Numerous experimental investigations have been performed since the 1960s to develop an understanding of the behavior of ceramics under high velocity impact and the behavior of the failed ceramic under high pressures [Wilkins et al. 1969; Shockey et al. 1990].

Recently, there has been interest in developing the capability to simulate the ballistic response of WC, which is widely used as a hard core in projectiles [Wilkins et al. 1969]. The cemented carbide utilized in [Burkins 2003] and in this analysis is comprised of 93% WC and 6% cobalt (the metallic binder). The modeling challenge lies in the ability to accurately represent the behavior of the WC core material. Several studies have been performed recently involving the impact of WC spheres on a variety of different target materials and thicknesses, and over a wide range of velocities [Williams 1995; Grady 1999]. However, few studies appear to have been performed on high velocity impact of HSLA steels. Martineau et al. [2004] examined experimentally and numerically the residual stress in the target HSLA material as a result of the WC sphere impact and subsequent cratering. The residual stress was examined because of its possible effect on the ability of armor or turbine blades to survive multiple impacts or to survive future service loads when the original impact event did not cause total failure.

The current investigation will test the existing material models of tungsten carbide and HSLA-100 steel by comparing available published experimental data [Martineau et al. 2004], such as the depth and diameter of the impact crater, against the corresponding simulated results. The simulation will use exclusively the SPH method for the WC projectile, and SPH and Lagrange methods for the HSLA-100 target. The response of the target to the impact will be analyzed by both discretization methods, SPH and Lagrange, for all the impact velocities in an effort to study the effect of these methods on the simulation accuracy. The commercially available finite element code, AUTODYN [2004] , will be used to simulate impact and penetration of HSLA-100 targets by WC projectiles. The contribution and sensitivity of the selected material parameters on the accuracy of the solution when compared to the experimentally determined results will be discussed in detail.

Details of the impact experiments have been reported by Martineau et al. [2004], and are summarized in Table 1. The 51 mm thick plate material was prepared by hot-cross-rolling. It was austenized at 900°C for 75 min and then water quenched. The tungsten carbide spheres were purchased from Machining Technologies, Inc. in Elmore, Ohio. The 6.35 mm diameter spheres, Grade 25, were composed of 94% WC with 6% a cobalt binder. The steel plate was impacted normal to the plate by the small diameter spheres with velocities ranging from 830–2550 m/s. For this study, the accuracy of the material models which were used to simulate the impact process will be established by comparing the simulated depth and width of the crater against the ones measured relative to the planar surface of the plate.

## 2. Numerical simulations

These twelve experiments were simulated using the nonlinear commercial analysis software AUTODYN [2004]. AUTODYN is a uniquely versatile explicit analysis tool for modeling the nonlinear dynamics

| | Grady Spall | | Mott Stochastic Failure | | Experimental | |
|---|---|---|---|---|---|---|
| Velocity (km/s) | Diameter | Depth | Diameter | Depth | Diameter | Depth |
| 0.83 | 6.3 | 6.01 | 7.55 | 5.38 | 6.35 | 4.57 |
| 0.97 | 7.18 | 7.18 | 7.92 | 5.32 | 6.60 | 5.59 |
| 0.98 | 7.44 | 7.24 | 8.00 | 5.55 | 6.53 | 5.46 |
| 1.27 | 8.6 | 8.21 | 8.38 | 7.31 | 7.49 | 7.09 |
| 1.28 | 8.67 | 8.55 | 8.67 | 7.38 | 7.29 | 6.86 |
| 1.50 | 9.2 | 8.9 | 9.32 | 8.84 | 8.00 | 8.51 |
| 1.81 | 10.4 | 10.1 | 10.66 | 11.19 | 8.92 | 8.79 |
| 1.91 | 11.08 | 10.48 | 11.19 | 11.86 | 9.27 | 8.53 |
| 2.15 | 12.0 | 11.3 | 11.82 | 12.98 | 9.91 | 8.41 |
| 2.22 | 13.22 | 11.4 | 12.00 | 13.11 | 10.03 | 8.64 |
| 2.46 | 13.9 | 11.73 | 12.56 | 12.48 | 10.87 | 9.5 |
| 2.55 | 13.34 | 11.81 | 13.14 | 13.62 | 11.43 | 9.6 |

**Table 1.** Impact velocity and resulting simulation crater diameter and depth (in mm) compared to the experimental data by Martineau et al. [2004]. The target was discretized using the SPH method.

of solids, fluids, gas and their interactions. We have successfully used AUTODYN software for the modeling of impact of metallic and ceramic targets.

Using the geometry detailed above, an axisymmetric model was generated for the analysis of the WC projectile and the HSLA-100 target. The HSLA-100 target was discretized using both methods, SPH with a particle size of 0.125 mm, and Lagrange with element size of 0.5 mm, respectively. The sphere was discretized using SPH with a particle size of 0.125 mm. The HSLA-100 target was modeled for all simulations using a shock equation of state (EOS) [Martineau et al. 2004], a Zerilli–Armstrong strength model [Hanson 2003], and a Johnson–Cook (equivalent plastic strain to failure) model using constants derived from the experimental results of Chae and Koss [2004] . Fitting constants to this data resulted in $D_1 = 0.0$, $D_2 = 4.8$, $D_3 = -2.7$, $D_4 = 0.01$, and $D_5 = 0.0$. The WC was modeled using a polynomial EOS [Holmquist et al. 2005], and a Johnson–Cook strength and failure model using constants from [Holmquist et al. 2005]. Nevertheless, initial results were disappointing; the WC appeared to fragment prematurely, and the results underestimated the depth-of-penetration (DOP) by 9% and overestimated the crater diameter by 50% at an impact velocity of 0.83 km/s. We then attempted to improve predictions of the WC fragmentation behavior by increasing the dynamic yield stress from $Y = 3$ GPa [Hanson 2003] to the value $Y = 4.95$ GPa reported in [Normandia 2004], and by evaluating two additional failure models: the Grady spall model, which was initially developed for spall in ductile metals [Grady and Kipp 1997], and the principal tensile failure strain model, with crack softening and stochastic failure [Mott 1947]. A summary of the constitutive properties of the HSLA-100 plate and the tungsten carbide spheres is given in Table 2. Analytical expressions of the material models are given in Appendix A.

The Grady spall model relates the spall stress $S$ in the ceramic to the dynamic yield stress and failure strain, $S = (2\rho c^2 Y \varepsilon_c)^{1/2}$, where $\rho$ is the mass density, $c^2 = E/\rho$ is the square of the wave speed in the material, and E is the modulus of elasticity of the material. We tried to improve the dynamic fragmentation behavior of the WC by using a larger value than the dynamic yield stress of $Y = 4.95$ GPa reported in [Normandia 2004], Young's modulus 620 GPa [Hanson 2003], and $\varepsilon_c = 0.0027$. Hence,

| Material | Description | Value | Units |
|---|---|---|---|
| HSLA plate | Density, $\rho$ | 7.842 | g/cm$^3$ |
| | Shear modulus | 76.3 | GPa |
| | Elastic modulus | 197.0 | GPa |
| | Yield stress | 103 | MPa |
| | Poisson's ratio | 0.29 | |
| | Grüneisen $\gamma$ | 2.17 | |
| WC spheres | Density, $\rho$ | 14.77 | g/cm$^3$ |
| | Shear modulus | 396 | GPa |
| | Bulk modulus | 362 | GPa |
| | Yield stress | 495 | MPa |
| | Principal tensile failure strain | 0.001 | |
| | Fracture energy | 40.32 | J/m$^2$ |

**Table 2.** Constitutive properties for the HSLA-100 plate and WC spheres.

the derived spall stress $S = 4$ GPa is only about 10% larger than the value reported by Grady [1999]; we note that Martineau et al. [2004] report failure strains of $\varepsilon_c = 0.015$ for WC, but this value would predict unrealistically high spall stresses in the WC (using the equation above). The spall stress S is then equated to the local maximum principal stress necessary for failure in AUTODYN.

The Mott stochastic failure model [Mott 1947] as implemented in AUTODYN is a probabilistic failure model used to simulate an initial flaw distribution (heterogeneity) in the material; we randomized the principal strain-to-failure in the ceramic about $\varepsilon_c = 0.001$, with stochastic variance $\xi = 100$, and crack-softening with fracture energy $G_f = 40.3\,\mathrm{J/m^2}$.

**2.1.** ***SPH method.*** The results of the simulations, where the HSLA-100 target was discretized by the SPH, are summarized in Table 1; despite the rather sophisticated modifications to the models of the failure behavior of the ceramic relative to that reported in [Martineau et al. 2004], the results did not correlate well with the experimental observations.

Figures 1 and 2 compare the simulation results of the crater diameter and depth to the experimentally obtained values with increasing impact velocity.

Both modeling efforts result in premature tungsten carbide failure. In general, the calculated penetration depth and crater diameter are overestimated when compared to the experimentally obtained values. The relationship between crater depth and experimental velocity is much more linear in numerical predictions than indicated by the experimental data. Martineau et al. [2004] also observed a similar trend of the crater evolution versus the impact velocity using LS-DYNA. They used a less sophisticated material and failure model for their simulations, but with qualitatively similar results. Figure 1 shows that for impact velocities from 830 to 2550 m/s both failure modeling approaches overpredicted the crater diameters by about 15%.

| | Grady Spall | | Mott Stochastic Failure | | Experimental | |
|---|---|---|---|---|---|---|
| Velocity (km/s) | Diameter | Depth | Diameter | Depth | Diameter | Depth |
| 0.83 | 6.26 | 4.31 | 5.4 | 4.44 | 6.35 | 4.57 |
| 0.97 | 6.82 | 5.58 | 6. | 5.89 | 6.60 | 5.59 |
| 0.98 | 6.82 | 6. | 5.84 | 5.94 | 6.53 | 5.46 |
| 1.27 | 7.58 | 7.13 | 7. | 7.78 | 7.49 | 7.09 |
| 1.28 | 7.8 | 8.41 | 7.04 | 7.78 | 7.29 | 6.86 |
| 1.50 | 8.16 | 8.53 | 8.00 | 9.05 | 8.00 | 8.51 |
| 1.81 | 9.04 | 8.59 | 8.24 | 9.13 | 8.92 | 8.79 |
| 1.91 | 9.3 | 9.21 | 9.1 | 9.18 | 9.27 | 8.53 |
| 2.15 | 10.38 | 8.64 | 9.74 | 10.33 | 9.91 | 8.41 |
| 2.22 | 10.56 | 8.64 | 10.8 | 10.72 | 10.03 | 8.64 |
| 2.46 | 10.56 | 9.51 | 10.9 | 10.6 | 10.87 | 9.5 |
| 2.55 | 11.58 | 9.87 | 11.82 | 10.34 | 11.43 | 9.6 |

**Table 3.** Impact velocity and resulting simulation crater diameter and depth (in mm) compared to the experimental data by Martineau et al. [2004]. The target was discretized using the Lagrange method.

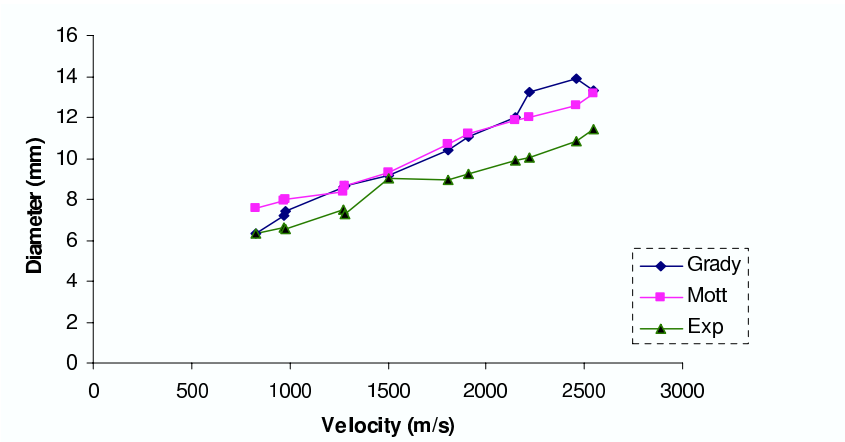


**Figure 1.** Comparison of crater diameter versus velocity for experimental data and numerical models, using SPH target discretization.

Figure 2 shows that the Mott failure model more closely predicted the DOP at velocities less than 1.5 km/s, but the Grady spall model performed better at velocities greater than 1.5 km/s. However, at the maximum impact velocity of 2.55 km/s, the Grady spall model overpredicted the DOP by 23%, whereas the Mott failure model overpredicted the DOP by 40%; this discrepancy is perhaps due to the fact that the published values were developed for the core of an armor piercing projectile, which is also composed of WC-6% Co, but may possess a different statistical strength, surface finish, and flaw/inclusion distribution than the WC-6% Co sphere utilized in the experiments being studied here. Indeed, more recent experimental efforts utilizing WC-6% Co spheres from a different manufacturer have resulted in the spheres fracturing at lower velocities than the velocities used in this paper [Fountzoulas et al. 2005]. Neither failure model was able to simulate the relative leveling-off of the penetration depth

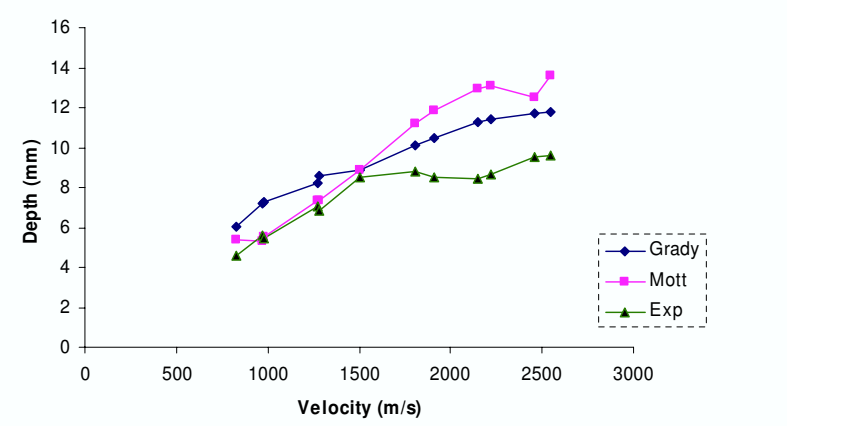


**Figure 2.** Comparison of crater depth versus velocity for experimental data and numerical models, using SPH target discretization.

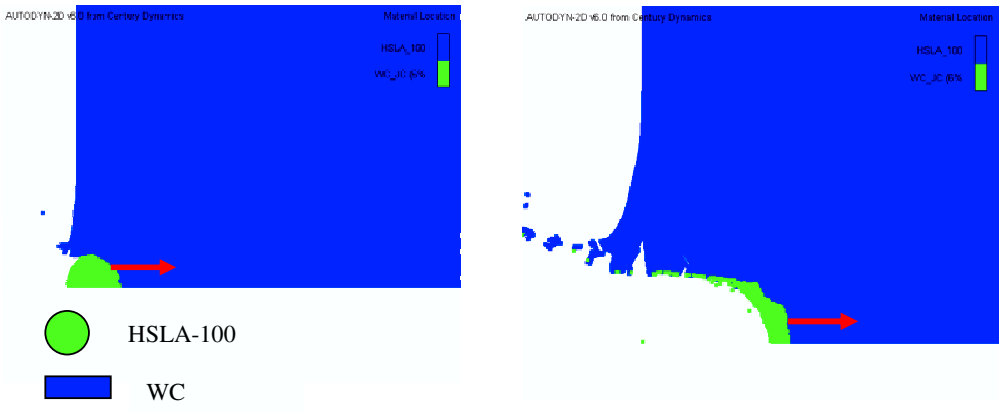


**Figure 3.** Impact at 830 m/s 22 $\mu$s (left). Impact at 2550 m/s, 22 $\mu$s (right).

between 1500–2250 m/s (Figure 2). Furthermore, this discrepancy may be attributed to the fact that the SPH method is employed mostly for ceramics simulation rather than ductile materials, such as metals.

Figure 3 shows the penetration of the HSLA-100 target at 22 $\mu$s for impact velocities of 830 and 2550 m/s. For the 2550 m/s impact velocity the simulation predicts disintegration of the WC sphere impactor and the region around the crater lip beginning to spall.

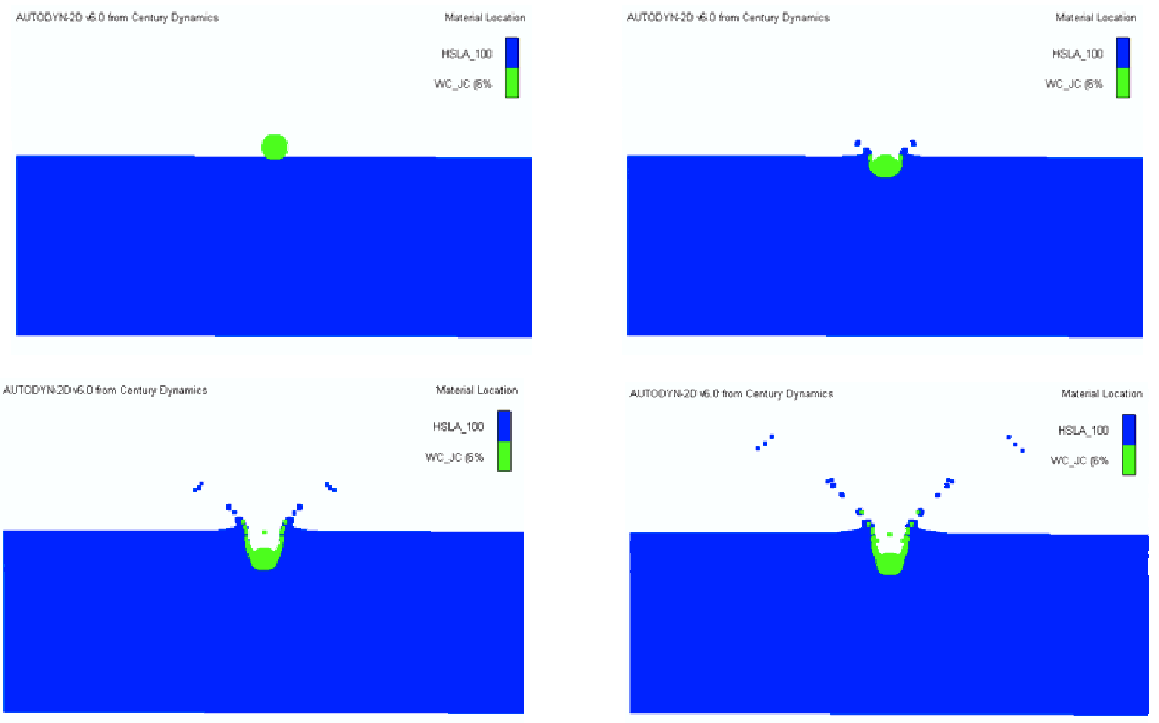

**Figure 4.** Section of the SPH elements illustrating projectile erosion and target penetration at 0 $\mu$s (upper left), 4 $\mu$s (upper right), 11 $\mu$s (lower left), and 22 $\mu$s (lower right).

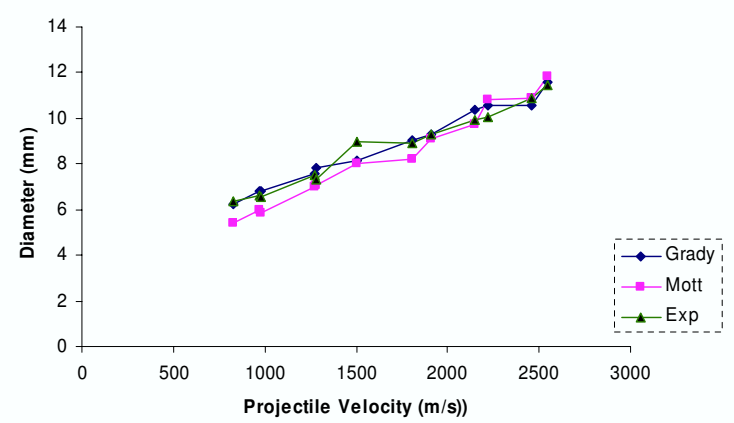


**Figure 5.** Comparison of crater diameter versus velocity for experimental data and numerical models, using Lagrangian discretization.

Figure 4 illustrates the erosion of the WC projectile and the penetration of the HSLA-100 target, using principal strain with crack softening and stochastic variation as the failure model of the target, for an impact velocity 1810 m/s.

**2.2.** ***Lagrangian method.*** The HSLA-100 target was discretized using the Lagrangian method with 0.5 mm element size. The results of the Lagrangian simulations are summarized in Table 3. As Figure 5 shows, the correlation of the simulation results and the experimental data for the crater diameter is excellent. The correlation of the simulation results and the experimental data for the crater depth is excellent for all velocities using the Grady failure model (Figure 6). However, as also illustrated in Figure 6, the Mott failure model did not result in similar excellent correction for the all impact velocities when compared to the crater diameter simulation results. Although the simulation results overestimate the crater depth for all the impact velocities, they are in reasonable agreement for impact velocities up

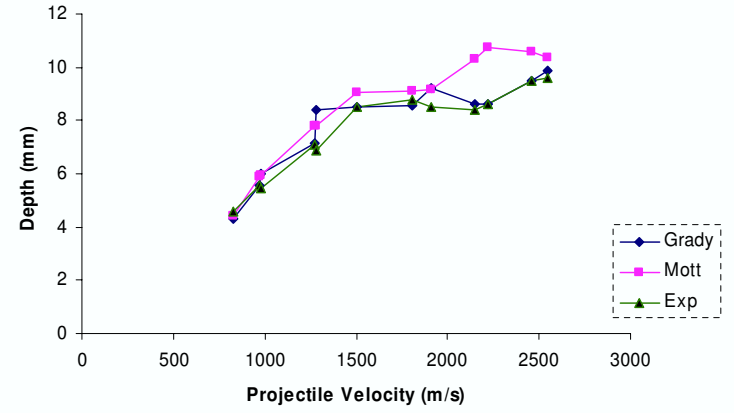


**Figure 6.** Comparison of crater depth versus velocity for experimental data and numerical models, using Lagrangian discretization.

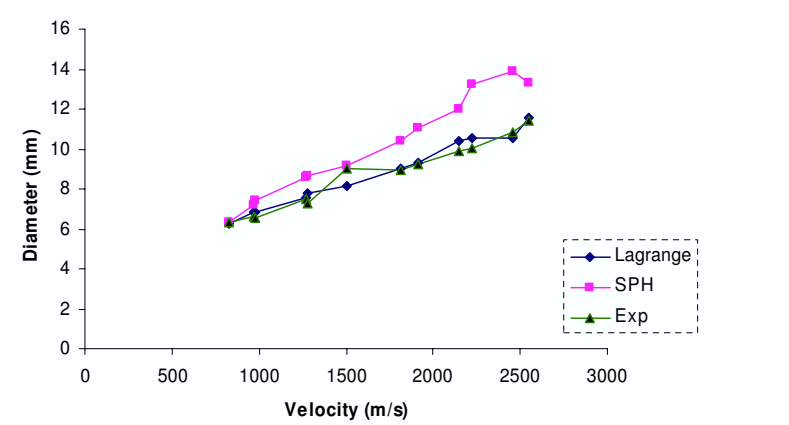


**Figure 7.** Comparison of experimental data for crater diameter with simulation results using SPH and Lagrangian discretization methods for steel target for Grady failure model for WC projectile

to 1810 m/s. As observed in both Figures 5 and 6, for impact velocities above 1810 m/s the simulation predictions overestimate the crater depth. However, it is worth mentioning that the experimental leveling-off of the penetration depth is followed by the Lagrange simulation method, unlike the SPH method.

The simulation differences between the SPH and Lagrange methods for both failure models of HSLA-100 target Grady criterion and Mott are illustrated in Figures 7–11. The Lagrange element erosion issue was overcome by turning on the *prevent erosion of degenerate cells* and *retain inertia or eroded nodes* option of the AUTODYN commercial software.

Figure 11 shows the erosion of the WC projectile and the penetration of the HSLA-100 target, using principal strain with crack softening and stochastic variation as the failure model of the target, for impact velocity 1810 m/s.

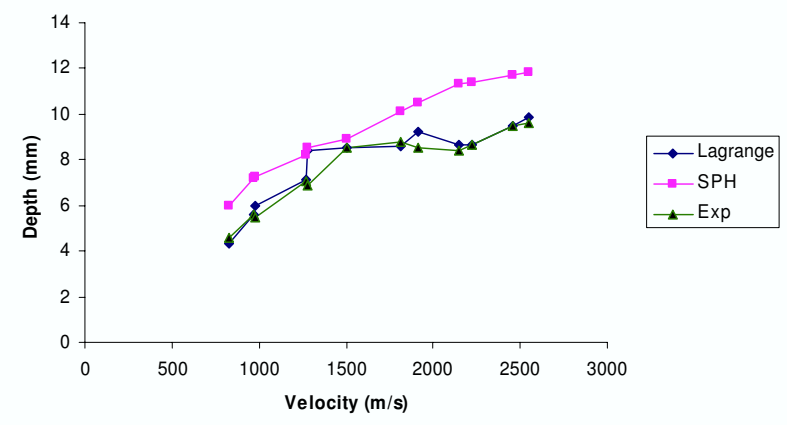


**Figure 8.** Comparison of experimental data for the crater depth with simulation results using SPH and Lagrangian discretization methods for steel target for Grady failure model for WC projectile.

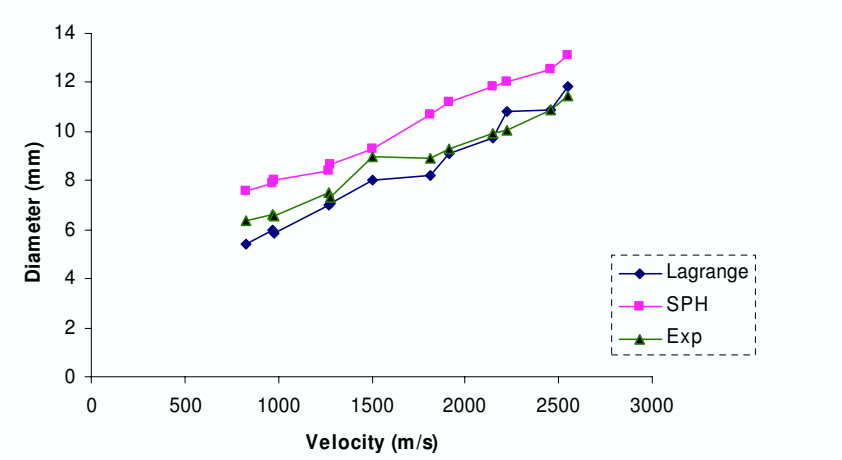


**Figure 9.** Comparison of experimental data for the crater diameter with simulation results using SPH and Lagrangian discretization methods for steel target for Mott stochastic variation failure model and principal strain for WC projectile.

## 3. Discussion

The ballistic behavior of an HSLA-100 target impacted by a WC sphere was simulated by discretizing it with two different methods, Lagrange and SPH. The SPH method, although it has been used successfully for ballistic simulation of ceramic materials, did not produce as accurate results as the Lagrangian method. The Grady failure model reproduced the experimental data of the crater diameter and depth more accurately for both the Lagrangian and SPH methods. The Lagrangian method reproduced the experimental data accurately, with the exception of the Mott failure, which showed small deviation from

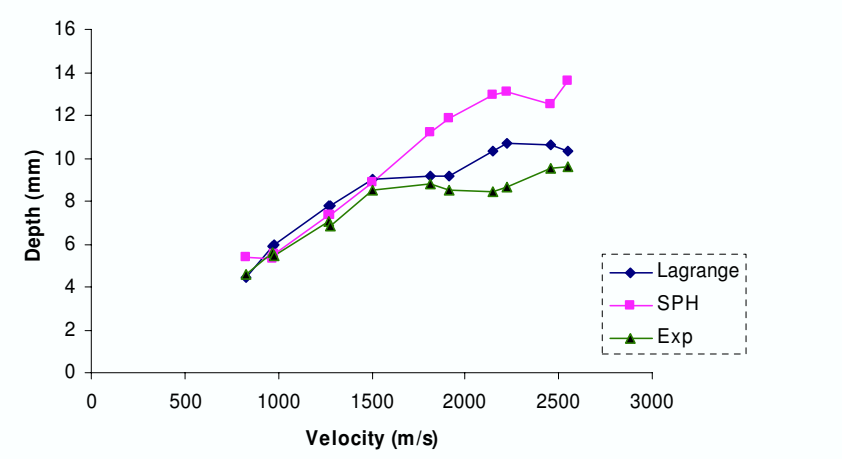


**Figure 10.** Comparison of experimental data for the crater depth with simulation results using SPH and Lagrangian discretization methods for steel target for Mott stochastic variation failure model and principal strain for WC projectile.

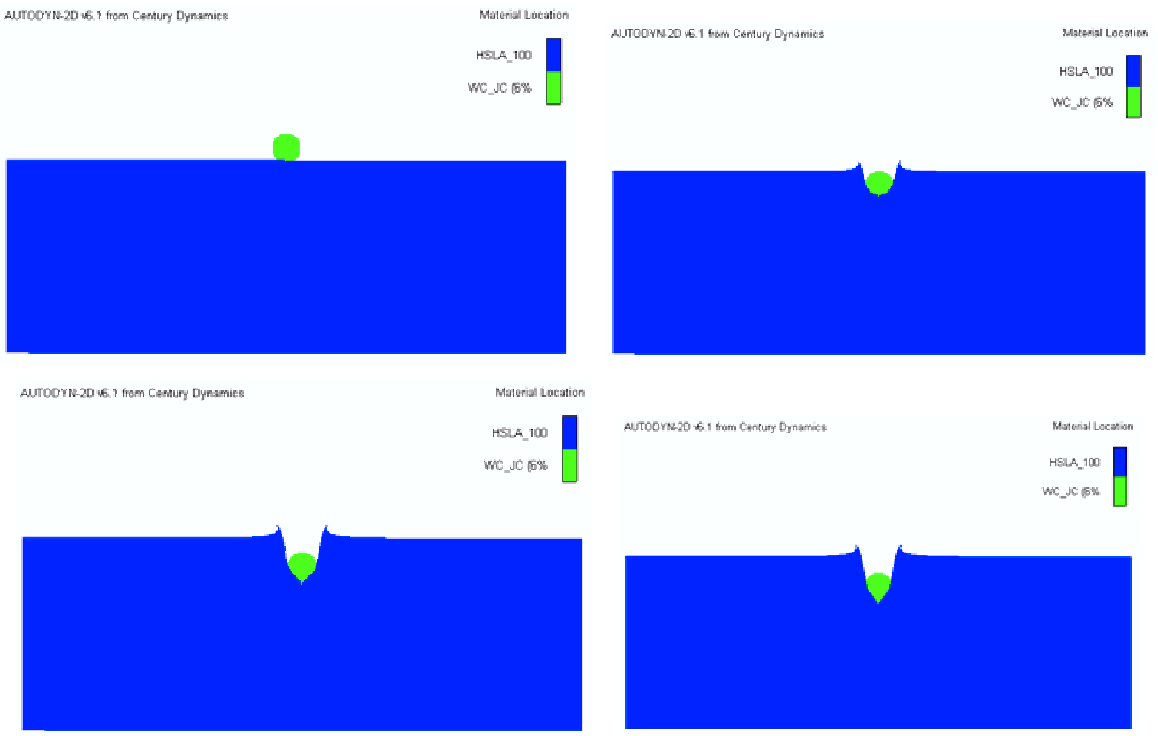


**Figure 11.** Section of the Lagrange elements illustrating projectile erosion and target penetration at 0 $\mu$s (upper left), 4 $\mu$s (upper right), 11 $\mu$s (lower left), and 22 $\mu$s (lower right).

the experimental data. To the authors' knowledge, targets meshed by the SPH method exhibit enhanced sensitivity to spall relative to targets meshed with the Lagrange method. The small deviation of the simulated values from the experimental values (Figures 5–10) may be attributed to: (a) an accurate material model for the WC; and (b) the parameters of the constitutive properties of the HSLA-100 target Johnson–Cook (equivalent plastic strain to failure) model were derived from the experimental results of Chae and Koss [2004] through interpolation of their experimental values. However, we believe that the derived constants resulted in a reasonably accurate failure model, and they did not contribute to the disagreement between the simulated and experimental data of the crater diameter and depth. Until the behavior of the tungsten carbide utilized in these sphere impact experiments can be accurately modeled, the current study on the applicability of the existing tungsten carbide strength and failure models to high velocity impact will remain incomplete.

However, a few salient points can be drawn. Although the Lagrangian method predicted the experimental values of the crater diameter and depth more accurately than the SPH method, the SPH method does reproduce accurately the failure of the ductile materials within acceptable statistical error. Precise knowledge of the HSLA-100 yield strength, mainly a function of manufacturing and heat treatment, is a significant factor in accurate simulation. Since the Zerilli–Armstrong strength model is limited by the strain-rate at which the maximum dislocation velocity is reached, prior knowledge of that strain-rate

is of great importance for accurate prediction of the target failure. The simulation results have shown that none of the WC failure models appear well calibrated for impact velocities over the entire range investigated (830 to 2550 m/s). However, the prediction of the leveling-off of the penetration depth is a convincing indication that the Lagrange discretization, in conjunction with the Grady failure model, is the indicated method of predicting the failure of HSLA-100 steel impacted by a tungsten carbide sphere. Finally, Hanson [2003] concludes that the Zerilli–Armstrong constitutive model does not account for the plastic behavior of HSLA-100 steel to better than 10%, and we are not aware of any detailed studies of the dynamic failure behavior of HSLA-100 steel which could, in part, be responsible for the discrepancies between the experimental and computed results reported herein.

## 4. Conclusion

This paper has illustrated some of the difficulties involved in modeling the complex fragmentation behavior of a tungsten carbide sphere impacting an HSLA-100 plate. The computational investigation tested some existing material and failure models of tungsten carbide and HSLA-100 steel by comparing available published experimental data, such as the depth and diameter of the impact crater, with simulation results. Generally speaking, the Lagrange discretization of the HSLA-100 plate utilizing the Grady failure model predicted the crater depth and diameter accurately. A finer particle size for the SPH method would not have necessarily predicted the experimental data more accurately, since SPH mesh convergence studies have shown that penetration depth is a nonmonotonic function of particle size. The Langrangian discretization method in conjunction with recent WC strength and WC failure models produced accurate agreement over the entire range of impact velocities investigated. However, previous work [Fountzoulas et al. 2005] that investigated the ability of existing computational models of WC spheres impacting confined SiC targets also concluded that more accurate WC failure models are needed if we are to make accurate predictions at high impact velocities.

## Appendix A

***Zerilli–Armstrong model*** The constitutive equation of this model is based on the dislocation theory mechanics [Thompson 2006]. This model attempts to better describe material behavior, as well to extrapolate beyond the strain-rates and temperatures seen in experiments.

Their constitutive model consists of a thermal and an a-thermal part, and introduces grain-size dependence.

$$\sigma = \sigma_{\text{thermal}} + \sigma_{\text{athermal}} + kl^{1/2}, \tag{A.1}$$

where

$$\sigma_{\text{thermal}} = B\exp(\beta T). \tag{A.2}$$

The thermal stress is the stress necessary to overcome thermally activated dislocation barriers. Thus, it increases as the strain-rate increases and decreases as the temperature increases. For FCC metals, the thermal activation energy is dependent on dislocation interactions. Since the dislocation density increases as the strain increases, the thermal portion of the stress is dependent on the strain, as well as the strain-rate and temperature.

$$\sigma_{\text{thermal-FCC}} = c_2\varepsilon^{1/2}\exp(-c_3T + c_4Tln\dot{\varepsilon}) \tag{A.3}$$

$$\sigma_{\text{thermal-BCC}} = c_1 \exp(-c_3 T + c_4 T ln\dot{\varepsilon}) \tag{A.4}$$

The final constitutive equation for BCC metals is shown in Equation (A.5), where $\sigma_0$ accounts for the grain size and initial yield strength,

$$\sigma = \sigma_{0+} c_1 \varepsilon^n + c_1 \exp(-c_3 T + c_4 T ln\dot{\varepsilon}). \tag{A.5}$$

Of note is that the Zerilli–Armstrong equations cannot be used for strain rates at which the maximum dislocation velocity is exceeded. Thus, the limit of extrapolation is the strain-rate at which the maximum dislocation velocity is reached.

**A.1** ***Johnson–Cook failure model*** Failure accumulation in the Johnson–Cook model does not directly degrade the yield surface [Johnson and Cook 1985; Kay 2003]. The model defines the strain at fracture as

$$\varepsilon_{\text{failure}} = [D_1 + D_2 \exp(D_3 \sigma^*)][1 + D_4 ln(\dot{\varepsilon}^*)][1 = T_5^*], \tag{A.6}$$

where $\sigma^*$ is the ratio of the pressure to the effective stress, that is,

$$\sigma^* = \text{Pressure}/\sigma_{\text{eff}}. \tag{A.7}$$

Fracture occurs in the Johnson–Cook model when the damage parameter D exceeds 1.0. The evolution of D is given by the accumulated incremental effective plastic strains divided by the current strain at fracture as

$$D = \Sigma \varepsilon_{\text{eff}}^P / \varepsilon_{\text{failure}}. \tag{A.8}$$

During the calculation, element stresses are all set to zero, and remain equal to zero when the fracture criteria is evoked for a specific element.

The first set of brackets in the Johnson–Cook fracture model are intended to represent the observation that the strain to fracture decreases as the hydrostatic tension increases. The second set of brackets in the strain to failure expression represent the effect of an increased strain rate on the material ductility, while the third set of brackets represent the effect of thermal softening on the material ductility.

**A.2** ***The Grady spall criterion*** An estimate of the critical spall stress of a ductile material can be made using the following formula due to Grady,

$$S = (2\rho c^2 Y \varepsilon_f)^{1/2}, \tag{A.9}$$

where $\rho$ is the density, c the bulk sound speed, Y the yield stress, and $\varepsilon_f$ is a critical strain failure usually set to 0.15 [AUTODYN 2004; Grady and Kipp 1997].

This spall stress is calculated for each cell at each cycle, thus including the local conditions in the cell. The calculated spall stress is used as the local maximum principal stress failure criterion in the cell.

**A.3** ***Stochastic failure*** The materials have inherent microscopic flaws, and these flaws are where the failure and cracking initiate. An approach to reproducing this numerically is to randomize the failure stress/strain for the material [Johnson and Cook 1985]. Therefore, each cell in the numerical model will

have a different failure strain, thus creating weak spots in the material. A Mott distribution is used to define the variance in failure stress/strain, as defined by

$$P = 1 - \exp[-(C/\gamma)e^{\gamma\varepsilon}], \tag{A.10}$$

where P is the probability of fracture; and C and $\gamma$ are constants. The constant C is calculated at failure stress/strain probability equal to 0.5, and $\gamma$ is defined by the user. The distribution type of P is defined by the value of $\gamma$; it can be either fixed, the same each type a part is filled, or random. The Mott distribution can be applied to most failure models.

## Acknowledgement

The authors wish to express their wholehearted gratitude to the reviewers whose productive criticism and suggestions made this paper better and more complete.

## References

[AUTODYN 2004] ANSYS, Inc., *AUTODYN theory manual*, Southpointe 275 Technology Drive Canonsburg, PA: ANSYS, Inc., 2004.

[Burkins 2003] M. Burkins, "An evaluation of 14.5 mm AP surrogate projectiles", Presented at the Ground Vehicle Survivability Symposium, 2003.

[Chae and Koss 2004] D. Chae and D. A. Koss, "Damage accumulation and failure of HSLA-100 steel", *Mater. Sci. Eng.* **366**:2 (2004), 299–309.

[Czyryca et al. 2003] E. J. Czyryca, D. P. Kihl, and R. DeNale, "Meeting the challenge of higher strength, lighter warships", *Amptiac Q.* **7**:3 (2003), 63–70.

[Fountzoulas et al. 2005] C. G. Fountzoulas, M. J. Normandia, J. C. LaSalvia, and B. A. Cheeseman, "Numerical simulations of silicon carbide tiles impacted by tungsten carbide spheres", 22nd International Symposium on Ballistics, 14–18 November 2005.

[Grady 1999] D. E. Grady, "Impact failure and fragmentation properties of tungsten carbide", *Int. J. Impact Eng.* **23**:1 (1999), 307–317.

[Grady and Kipp 1997] D. E. Grady and M. E. Kipp, "Fragmentation properties of metals", *Int. J. Impact Eng.* **20**:1-5 (1997), 293–308.

[Hanson 2003] K. Hanson, "Inference of material-model parameters from experimental data", LANL, 12 May 2003, Available at http://www.lanl.gov/home/kmh.

[Holmquist et al. 2005] T. J. Holmquist, G. R. Johnson, and W. A. Gooch, "Modeling the 14.5 mm BS41 projectile for ballistic impact computations", Presented at the 2nd International Conference on Computational Ballistics, 18–20 May 2005.

[Johnson and Cook 1985] G. R. Johnson and W. H. Cook, "Fracture characteristics of three metals subjected to various strains, strain rates, temperatures and pressures", *Eng. Fract. Mech.* **21**:1 (1985), 31–48.

[Kay 2003] G. Kay, "Failure modeling of Titanium 6Al-4V and aluminum 2024-T3 with the Johnson-Cook material model", Technical report, Washington, DC, 2003. DOT/FAA/AR-03/57.

[Martineau et al. 2004] R. L. Martineau, M. B. Prime, and T. Duffey, "Penetration of HSLA-100 steel with tungsten carbide spheres at striking velocities between 0.8 and 2.5 km/s", *Int. J. Impact Eng.* **30**:5 (2004), 505–520.

[Mott 1947] N. F. Mott, "Fragmentation of shell cases", pp. 300–308 in *Proceedings of the Royal Society of London*, vol. 189, Series A, Mathematical and Physical Sciences **1018**, 1947.

[Normandia 2004] M. J. Normandia, "Impact response and analysis of several silicon carbides", *Int. J. Appl. Ceram. Technol.* **1**:3 (2004), 226–234.

[Shockey et al. 1990] D. A. Shockey, A. H. Marchand, S. R. Skaggs, G. E. Cort, M. W. Burkett, and R. Parker, "Failure phenomenology of confined ceramic targets and impacting rods", *Int. J. Impact Eng.* **9**:3 (1990), 263–275.

[Thompson 2006] A. C. Thompson, "High strain rate characterization of advanced high strength steels", MS Thesis, University of Waterloo, Waterloo, Ontario, Canada, 2006.

[Wilkins et al. 1969] M. L. Wilkins, C. F. Cline, and C. A. Honodel, "Light Armor", Technical report UCRL-71817, Lawrence Radiation Laboratory, Livermore, CA, July 23 1969.

[Williams 1995] A. E. Williams, "The effect of phase changes on target response", *Int. J. Impact Eng.* **17**:4-6 (1995), 937–947.

Received 27 Jun 2007. Accepted 21 Aug 2007.

COSTAS G. FOUNTZOULAS: cfount@arl.army.mil
*U.S. Army Research Laboratory, Weapons and Materials Directorate, 2800 Powder Mill Rd, Adelphi, MD 20783-1197, United States*

GEORGE A. GAZONAS: gazonas@arl.army.mil
*U.S. Army Research Laboratory, Weapons and Materials Directorate, 2800 Powder Mill Rd, Adelphi, MD 20783-1197, United States*

BRYAN A. CHEESEMAN: bcheesem@arl.army.mil
*U.S. Army Research Laboratory, Weapons and Materials Directorate, 2800 Powder Mill Rd, Adelphi, MD 20783-1197, United States*